POLITECNICO DI TORINO
Repository ISTITUZIONALE

Low temperature direct growth of graphene patterns on flexible glass substrates catalysed by a sacrificial ultrathin Ni film

(Article begins on next page)

25 April 2024

Low temperature direct growth of graphene patterns on flexible glass substrates catalysed by a sacrificial ultrathin Ni film

MIRIAM MARCHENA,[1] DAVIDE JANNER,[1] TONG LAI CHEN,[1] VITTORIA FINAZZI,[1] AND VALERIO PRUNERI[1,2]

[1]ICFO–Institut de Ciències Fotòniques, The Barcelona Institute of Science and Technology, 08860 Castelldefels (Barcelona), Spain
[2]ICREA–Institució Catalana de Recerca i Estudis Avançats, Passeig Lluís Companys 23, 08010 Barcelona, Spain
*miriam.marchena@icfo.es

Abstract: Direct deposition of graphene on substrates would avoid costly, time consuming and defect inducing transfer techniques. In this paper we used ultrathin films of Ni, with thickness ranging from 5 to 50 nm, as a catalytic surface on glass to seed and promote chemical vapor deposition (CVD) of graphene. Different regimes and dynamics were studied for various parameters including temperature and reaction time. When a critical temperature (700 °C) was reached, Ni films retracted and holes formed that are open to the glass surface, where graphene deposited. After CVD, the residual Ni could be etched away and the glass substrate with graphene regained maximum transparency (>90%). The fact that we could achieve low growth temperatures indicates the potential of the technique to widen the range of substrate materials over which graphene can be directly deposited. We demonstrated this by depositing graphene patterns on ultrathin, 100 μm thick, sheet of glass with low strain point (670 °C), particularly suitable for flexible electronic and optoelectronic devices.

References and links

1. A. K. Geim and K. S. Novoselov, "The rise of graphene," Nat. Mater. **6**(3), 183–191 (2007).
2. Y. Hernandez, V. Nicolosi, M. Lotya, F. M. Blighe, Z. Sun, S. De, I. T. McGovern, B. Holland, M. Byrne, Y. K. Gun'Ko, J. J. Boland, P. Niraj, G. Duesberg, S. Krishnamurthy, R. Goodhue, J. Hutchison, V. Scardaci, A. C. Ferrari, and J. N. Coleman, "High-yield production of graphene by liquid-phase exfoliation of graphite," Nat. Nanotechnol. **3**(9), 563–568 (2008).
3. A. B. Bourlinos, V. Georgakilas, R. Zboril, T. A. Steriotis, and A. K. Stubos, "Liquid-phase exfoliation of graphite towards solubilized graphenes," Small **5**(16), 1841–1845 (2009).
4. X. Li, G. Zhang, X. Bai, X. Sun, X. Wang, E. Wang, and H. Dai, "Highly conducting graphene sheets and Langmuir-Blodgett films," Nat. Nanotechnol. **3**(9), 538–542 (2008).
5. D. Li, M. B. Müller, S. Gilje, R. B. Kaner, and G. G. Wallace, "Processable aqueous dispersions of graphene nanosheets," Nat. Nanotechnol. **3**(2), 101–105 (2008).
6. S. Stankovich, R. D. Piner, X. Chen, N. Wu, S. T. Nguyen, and R. S. Ruoff, "Stable aqueous dispersions of graphitic nanoplatelets via the reduction of exfoliated graphite oxide in the presence of poly(sodium 4-styrenesulfonate)," J. Mater. Chem. **16**(2), 155–158 (2006).
7. S. Stankovich, D. A. Dikin, R. D. Piner, K. A. Kohlhaas, A. Kleinhammes, Y. Jia, Y. Wu, S. T. Nguyen, and R. S. Ruoff, "Synthesis of graphene-based nanosheets via chemical reduction of exfoliated graphite oxide," Carbon **45**(7), 1558–1565 (2007).
8. V. C. Tung, M. J. Allen, Y. Yang, and R. B. Kaner, "High-throughput solution processing of large-scale graphene," Nat. Nanotechnol. **4**(1), 25–29 (2009).
9. S. Bae, H. Kim, Y. Lee, X. Xu, J. S. Park, Y. Zheng, J. Balakrishnan, T. Lei, H. R. Kim, Y. I. Song, Y. J. Kim, K. S. Kim, B. Özyilmaz, J. H. Ahn, B. H. Hong, and S. Iijima, "Roll-to-roll production of 30-inch graphene films for transparent electrodes," Nat. Nanotechnol. **5**(8), 574–578 (2010).
10. C. Mattevi, H. Kim, and M. Chhowalla, "A review of chemical vapour deposition of graphene on copper," J. Mater. Chem. **21**(10), 3324–3334 (2011).

11. Q. Yu, J. Lian, S. Siriponglert, H. Li, Y. P. Chen, and S.-S. Pei, "Graphene segregated on Ni surfaces and transferred to insulators," Appl. Phys. Lett. **93**(11), 113103 (2008).

12. Y. Zhang, L. Gomez, F. N. Ishikawa, A. Madaria, K. Ryu, C. Wang, A. Badmaev, and C. Zhou, "Comparison of Graphene Growth on Single-Crystalline and Polycrystalline Ni by Chemical Vapor Deposition," J. Phys. Chem. Lett. **1**(20), 3101–3107 (2010).

13. A. Reina, X. Jia, J. Ho, D. Nezich, H. Son, V. Bulovic, M. S. Dresselhaus, and J. Kong, "Large area, few-layer graphene films on arbitrary substrates by chemical vapor deposition," Nano Lett. **9**(1), 30–35 (2009).

14. H. Kim, I. Song, C. Park, M. Son, M. Hong, Y. Kim, J. S. Kim, H. J. Shin, J. Baik, and H. C. Choi, "Copper-vapor-assisted chemical vapor deposition for high-quality and metal-free single-layer graphene on amorphous SiO₂ substrate," ACS Nano **7**(8), 6575–6582 (2013).

15. P. S. Rusakov, I. I. Kondrashov, M. G. Rybin, A. S. Pozharov, and E. D. Obraztsova, "Chemical Vapor Deposition of graphene on copper foils," J. Nanoelectron. Optoelectron. **8**(1), 79–82 (2013).

16. I. Vlassiouk, P. Fulvio, H. Meyer, N. Lavrik, S. Dai, P. Datskos, and S. Smirnov, "Large scale atmospheric pressure chemical vapor deposition of graphene," Carbon **54**, 58–67 (2013).

17. A. Ismach, C. Druzgalski, S. Penwell, A. Schwartzberg, M. Zheng, A. Javey, J. Bokor, and Y. Zhang, "Direct chemical vapor deposition of graphene on dielectric surfaces," Nano Lett. **10**(5), 1542–1548 (2010).

18. S. J. Chae, F. Güneş, K. K. Kim, E. S. Kim, G. H. Han, S. M. Kim, H.-J. Shin, S.-M. Yoon, J.-Y. Choi, M. H. Park, C. W. Yang, D. Pribat, and Y. H. Lee, "Synthesis of large-area graphene layers on poly-nickel substrate by chemical vapor deposition: wrinkle formation," Adv. Mater. **21**(22), 2328–2333 (2009).

19. I. I. Kondrashov, P. S. Rusakov, M. G. Rybin, A. S. Pozharov, and E. D. Obraztsova, "Chemical Vapor Deposition of Graphene on Nickel from Different Gaseous Atmospheres," J. Nanoelectron. Optoelectron. **8**(1), 83–86 (2013).

20. J. Lahiri, T. S. Miller, A. J. Ross, L. Adamska, I. I. Oleynik, and M. Batzill, "Graphene growth and stability at nickel surfaces," New J. Phys. **13**(2), 025001 (2011).

21. C.-M. Seah, S.-P. Chai, and A. R. Mohamed, "Mechanisms of graphene growth by chemical vapour deposition on transition metals," Carbon **70**, 1–21 (2014).

22. R. S. Edwards and K. S. Coleman, "Graphene film growth on polycrystalline metals," Acc. Chem. Res. **46**(1), 23–30 (2013).

23. J. H. Warner, F. Schäffel, A. Bachmatiuk, and M. H. Rümmeli, *Graphene: Fundamentals and Emergent Applications* (Elsevier, 2013).

24. K.-J. Peng, C.-L. Wu, Y.-H. Lin, Y.-J. Liu, D.-P. Tsai, Y.-H. Pai, and G.-R. Lin, "Hydrogen-free PECVD growth of few-layer graphene on an ultra-thin nickel film at the threshold dissolution temperature," J. Mater. Chem. C Mater. Opt. Electron. Devices **1**(24), 3862–3870 (2013).

25. Y. Zhang, L. Zhang, and C. Zhou, "Review of chemical vapor deposition of graphene and related applications," Acc. Chem. Res. **46**(10), 2329–2339 (2013).

26. D. Q. McNerny, B. Viswanath, D. Copic, F. R. Laye, C. Prohoda, A. C. Brieland-Shoultz, E. S. Polsen, N. T. Dee, V. S. Veerasamy, and A. J. Hart, "Direct fabrication of graphene on SiO₂ enabled by thin film stress engineering," Sci. Rep. **4**, 5049 (2014).

27. R. Addou, A. Dahal, P. Sutter, and M. Batzill, "Monolayer graphene growth on Ni(111) by low temperature chemical vapor deposition," Appl. Phys. Lett. **100**(2), 021601 (2012).

28. A. Dahal and M. Batzill, "Graphene-nickel interfaces: a review," Nanoscale **6**(5), 2548–2562 (2014).

29. T. Hallam, N. C. Berner, C. Yim, and G. S. Duesberg, "Strain, bubbles, dirt, and folds: a study of graphene polymer-assisted transfer," Adv. Mater. Interfaces **1**(6), 1400115–1400121 (2014).

30. T. L. Chen, D. S. Ghosh, M. Marchena, J. Osmond, and V. Pruneri, "Nanopatterned Graphene on a Polymer Substrate by a Direct Peel-off Technique," ACS Appl. Mater. Interfaces **7**(10), 5938–5943 (2015).

31. H. Wang and G. Yu, "Direct CVD Graphene Growth on Semiconductors and Dielectrics for Transfer-Free Device Fabrication," Adv. Mater. Published ahead of print (2016).

32. T. Kaplas, D. Sharma, and Y. Svirko, "Few-layer graphene synthesis on a dielectric substrate," Carbon N. Y. **50**(4), 1503–1509 (2012).

33. C.-Y. Su, A.-Y. Lu, C.-Y. Wu, Y. T. Li, K.-K. Liu, W. Zhang, S.-Y. Lin, Z.-Y. Juang, Y.-L. Zhong, F.-R. Chen, and L.-J. Li, "Direct formation of wafer scale graphene thin layers on insulating substrates by chemical vapor deposition," Nano Lett. **11**(9), 3612–3616 (2011).

34. J. Kwak, J. H. Chu, J.-K. Choi, S.-D. Park, H. Go, S. Y. Kim, K. Park, S.-D. Kim, Y.-W. Kim, E. Yoon, S. Kodambaka, and S.-Y. Kwon, "Near room-temperature synthesis of transfer-free graphene films," Nat. Commun. **3**, 645 (2012).

35. M. Kosaka, S. Takano, K. Hasegawa, and S. Noda, "Direct synthesis of few- and multi-layer graphene films on dielectric substrates by "etching-precipitation" method," Carbon **82**, 254–263 (2015).

36. J. Sun, Y. Chen, M. K. Priydarshi, Z. Chen, A. Bachmatiuk, Z. Zou, Z. Chen, X. Song, Y. Gao, M. H. Rümmeli, Y. Zhang, and Z. Liu, "Direct Chemical Vapor Deposition-Derived Graphene Glasses Targeting Wide Ranged Applications," Nano Lett. **15**(9), 5846–5854 (2015).

37. J. Sun, Y. Chen, X. Cai, B. Ma, Z. Chen, M. K. Priydarshi, K. Chen, T. Gao, X. Song, Q. Ji, X. Guo, D. Zou, Y. Zhang, and Z. Liu, "Direct low-temperature synthesis of graphene on various glasses by plasma-enhanced chemical vapor deposition for versatile, cost-effective electrodes," Nano Res. **8**(11), 3496–3504 (2015).

38. S. Giurgola, A. Rodriguez, L. Martinez, P. Vergani, F. Lucchi, S. Benchabane, and V. Pruneri, "Ultra thin nickel transparent electrodes," J. Mater. Sci. Mater. Electron. **20**(1), 181–184 (2009).

39. L. Martínez, D. S. Ghosh, S. Giurgola, P. Vergani, and V. Pruneri, "Stable transparent Ni electrodes," Opt. Mater. **31**(8), 1115–1117 (2009).
40. B. O'Connor, C. Haughn, K.-H. An, K. P. Pipe, and M. Shtein, "Transparent and conductive electrodes based on unpatterned, thin metal films," Appl. Phys. Lett. **93**(22), 223304 (2008).
41. C. V. Thompson, "Solid-state dewetting of thin films," Annu. Rev. Mater. Res. **42**(1), 399–434 (2012).
42. P. R. Gadkari, P. Warren, R. M. Todi, R. V. Petrova, and K. R. Coffey, "Comparison of the agglomeration behavior of thin metallic films on SiO₂," J. Vac. Sci. Technol. A **23**(4), 1152 (2005).
43. L. Baraton, Z. B. He, C. S. Lee, C. S. Cojocaru, M. Châtelet, J.-L. Maurice, Y. H. Lee, and D. Pribat, "On the mechanisms of precipitation of graphene on nickel thin films," EPL **96**(4), 46003 (2011).
44. A. Delamoreanu, C. Rabot, C. Vallee, and A. Zenasni, "Wafer scale catalytic growth of graphene on nickel by solid carbon source," Carbon **66**, 48–56 (2014).
45. L. L. Patera, C. Africh, R. S. Weatherup, R. Blume, S. Bhardwaj, C. Castellarin-Cudia, A. Knop-Gericke, R. Schloegl, G. Comelli, S. Hofmann, and C. Cepek, "In situ observations of the atomistic mechanisms of Ni catalyzed low temperature graphene growth," ACS Nano **7**(9), 7901–7912 (2013).
46. A. C. Ferrari, J. C. Meyer, V. Scardaci, C. Casiraghi, M. Lazzeri, F. Mauri, S. Piscanec, D. Jiang, K. S. Novoselov, S. Roth, and A. K. Geim, "Raman spectrum of graphene and graphene layers," Phys. Rev. Lett. **97**(18), 187401 (2006).
47. L. M. Malard, M. A. Pimenta, G. Dresselhaus, and M. S. Dresselhaus, "Raman spectroscopy in graphene," Phys. Rep. **473**(5–6), 51–87 (2009).
48. A. C. Ferrari and D. M. Basko, "Raman spectroscopy as a versatile tool for studying the properties of graphene," Nat. Nanotechnol. **8**(4), 235–246 (2013).
49. J. Yoo, S. P. Patole, and H. Lee, "Method for fabricating three dimensional graphene structures using catalyst templates," United States Patent, US 8663593 B2 (2014).
50. S. Garner, S. Glaesemann, and X. Li, "Ultra-slim flexible glass for roll-to-roll electronic device fabrication," Appl. Phys., A Mater. Sci. Process. **116**(2), 403–407 (2014).

1. Introduction

Since graphene was first isolated in 2004 by A. Geim and K. Novoselov [1] using the mechanical exfoliation technique, its unique properties have made it one of the most studied materials. It has a wide range of potential applications, including in electronic and photonic industries. There is thus a need of obtaining large and uniform layers on insulating (dielectric) substrates, preferably by direct growth and synthesis and avoid in this way time consuming, cumbersome and not always defect-free transfer techniques.

Chemical and non-chemical exfoliation from graphite [2–4], chemical reduction of graphene oxide [5–8] and chemical vapor deposition (CVD) [9–13] have been investigated as techniques to produce graphene sheets. CVD has the potential of great versatility and high process yield for production of high quality graphene over large areas [14]. With such technique, graphene synthesis is typically obtained by employing transition catalytic metals in order to reduce the activation energy of carbon decomposition from a hydrocarbon gas [10,15–21]. Among the possible catalysts [22], the two most widely employed are Cu and Ni, each producing a different mechanism depending on the carbon solubility. Carbon has a low solubility in Cu and it is adsorbed only on the surface [23], whereas it is highly soluble in Ni where, after absorption, it diffuses through the metal and eventually post-segregate on the surface [21,23–25]. The highest quality CVD graphene has been obtained on μm-thick Cu foils [9] due to the fact that carbon atoms remain on the catalyst surface and single layer graphene (SLG) sheets are easily grown. Instead, on Ni foils, multilayer graphene (MLG) mostly grows with poor control on the number of layers [11]. On thin Ni films of a thickness 150-200 nm, a partial coverage with SLG has been obtained although mixed with MLG that starts its growth preferentially at the grain boundaries of the metal [13,26–28].

After growth, graphene has to be transferred from the metal to any target substrate and this is usually done by using a polymer assisted transfer technique that tends to leave residues and contamination which have a detrimental effect on its electrical and mechanical properties [14,29]. Several polymer-free transfer techniques are being developed but quality, performance of the resulting graphene and process scalability are not always adequate for device applications [30]. A more efficient alternative is to avoid completely the transfer and directly grow graphene on target substrates. A recent review has been published which covers some of the work on direct growth of graphene [31]. Initial results have been obtained by

using Cu in vapor phase as a catalyst but with poor coverage [14]. In refs [17,32]. a metal film of Cu deposited on a glass substrate was used to promote and catalyse graphene growth. During CVD, the Cu film retracted and dewetted as a consequence of the high temperatures, leaving behind regions of the substrate surface covered by graphene. The thicknesses of Cu films used in ref [32]. was in the 100-300 nm range while the films in ref [17]. were always significantly thick (>100 nm). In addition, the process required high temperature (1000 °C) and long duration (5-7 hours) for achieving dewetting and partial evaporation of Cu, which poses a practical limitation in large scale production. The method could be applied only to glass substrates with high strain point, such as fused silica. Also, a large portion of the Cu film remained on the substrate after completion of the process, resulting in poor transparency for the graphene on glass structure. In a subsequent work the remaining Cu was etched and a larger transparency was achieved [33]. Interestingly, Ni combined with carbon powder was also used to grow nanocrystalline graphene on glass and plastic substrates at 25-260°C [34]. More recently, a technique to directly grow graphene on dielectrics at low temperatures (600°C) was proposed [35]. The method used Fe-C solid solutions where carbon precipitates after the metal is etched away by Cl_2 gas during 30 minutes. Such an approach produces few- and multi-layer graphene but not SLG. Ref [36]. reports homogeneous direct growth of graphene on glass by CVD technique using high temperatures (1000-1100°C) and reaction times of 1-7 hours, these conditions being not suitable for a wide range of substrates. Plasma Enhanced CVD (PECVD) has been used in ref [37]. to directly grow few and multilayer graphene at low temperatures (400-600°C).

In this paper, we propose to use ultra-thin metal films (UTMFs) [38–40] of Ni to catalyse, seed and promote the growth of graphene on dielectric substrates. With respect to ref [17], our work made use of much thinner (5-50 nm) metal films, Ni instead of Cu, leading to significantly lower processing temperatures, times and metal residues. Also, by systematically studying and controlling the dewetting behaviour during the CVD growth, we achieved large substrate areas with graphene at 700°C and for 30 minutes. After chemically removing the Ni residues of the CVD growth, the optical transmittance of the graphene on substrate structure was >90%, only about 2.5% less than the bare glass substrate. We also deposited patterns of graphene starting from predefined Ni UTMF geometries, this being an essential feature for the functionality of many devices. The low temperature and short processing time were essential to achieve direct growth of graphene on flexible substrates of Corning® Willow® Glass, which has a low strain point (670°C), demonstrating the potential of the proposed techniques for transparent flexible electronics.

2. Experimental

2.1 Sample preparation

The substrates employed are flat fused silica, SiO_2/Si and Willow® Glass (see the Appendix for additional details). After organic cleaning by sonication (acetone and isopropanol), different thicknesses of thin layers of Ni were deposited by magnetron sputtering (Ar atmosphere at room temperature) preceded by a 120 seconds Ar plasma pre-treatment (8 mTorr, 40 W) in the same chamber.

On Ni covered substrates, graphene was grown by means of CVD (Black Magic 4-inch, AIXTRON: CH_4/H_2: 30/20 sccm, 7 mbar, and 50-75°C/min heating/cooling rates) at different temperatures, from 700°C to 1000°C, in steps of 100°C. Lower temperatures would not be sufficient for the endothermic CH_4 decomposition reaction to occur.

For all samples presented in section 4, after graphene growth, a 5 to 15 minutes dipping in diluted aqua regia (1:2:2 HCl: HNO_3: H_2O) was performed to remove the dewetted Ni nanoparticles remaining on the surface. For patterning the samples on Si/SiO_2 and willow glass substrates, a first lithography step using laser writer (LaserWriter LW405B, MICROTECH) was performed after spin coating a photoresist, followed by Ni deposition and

lift-off. For electrical measurements, a second lithography was carried out to deposit Au contacts.

2.2 Sample characterization

Surface topography of the samples was studied by Atomic Force Microscopy (AFM, Bruker/Veeco Dimension 3100) and FEI-Scanning Electron Microscopy (FE-SEM, FEI Inspect F). Structural characterization was carried out by grazing incidence X-ray diffraction (GXRD) and Raman spectroscopy (Renishaw inVia). GXRD was performed using Cu K radiation and a Philips MRD goniometer equipped with four crystal Bartels Ge 220 monochromator. Raman measurements were carried out with a 532 nm laser and a 100X objective lens for shifts ranging from 1100 to 2900 cm^{-1}. Raman maps were also acquired in order to get a statistical overview of the whole samples, with the mean value and standard deviation of at least 10 measurements at different sample's locations. Sheet resistance measurements (Rs) were carried out using a 4-point probe equipment. Rs values in section 3 correspond to samples where Ni particles still remain on the substrate (immediately measured after CVD). Rs values in section 4 correspond to samples where Ni was removed through etching. Chemical characterization was performed by energy-dispersive X-ray spectroscopy (EDX, Oxford INCA) after dipping samples in aqua regia to confirm that Ni residual nanoparticles have been removed. EDX measurements were also carried at 10 different points using 10 kV voltage.

3. Results and discussion

3.1 Ni dewetting

Within the working temperature range (700-1000°C) and pressure (7 mbar) of our study, Ni is well below its melting point, so it remains in solid state, but for the low thicknesses considered here, it dewets. This makes possible to grow graphene in a specific position, where Ni is initially sputtered, and, at the same time, in direct contact with the substrate surface, thanks to the subsequent Ni retraction. In this way one can avoid transfer from the growth to the final substrate. The retraction velocity of the metal and holes formation in the film strongly depend on temperature and initial film thickness. While single crystal Ni films dewetting on oxides surfaces (e.g. MgO) has been widely investigated [41], not much investigation has been devoted to the study of polycrystalline Ni films dewetting (≤50 nm). Specifically, two parameters proved to be crucial: the retraction velocity and the temperature at which dewetting starts ($T_{dewetting}$). Figure 9 (in Appendix) shows experimental results of $T_{dewetting}$ as a function of Ni film thickness, obtained at similar conditions and using criteria as in previous studies for other materials (e.g. Cu) [41,42], i.e. $T_{dewetting}$ was assumed as the temperature corresponding to which 5% of a 1 μm^2 substrate area is uncovered. The results indicate that, thanks to the small thicknesses used in this work (5, 15 and 50 nm), all films should dewet within 700-1000°C except for the 50 nm one processed at 700°C, where only small holes should form in the film.

3.2 Graphene growth

Graphene quality is highly dependent on the surface properties of the substrate (in our case Ni UTMF), including the crystal orientation, that affect carbon gas dehydrogenation, adsorption, surface diffusion and generation of H_2 [23,43,44]. To characterize the deposited Ni films and the structural modification it undergoes during the process, we used GXRD analysis. In Fig. 1, a significant difference in crystallinity can be observed between as-sputtered Ni UTMF of 50 nm and the same film after CVD treatment.

   During the heating phase of the process, Ni grains increase in size producing a polycrystalline structure in which their size becomes of the order of a few hundred nanometers. The crystallinity of the film shows preferential orientations along the (111) and

(220) planes. The (111) crystal orientation promotes SLG nucleation due to matching in crystal lattice structure and dimensions [27,45]. A relatively weak peak at $2\theta = 25.4°$ ascribable to graphene [44] is also present after CVD growth. Process conditions for the growth were kept fixed except for the temperature and reaction time, which were varied from 700°C to 1000°C and from 15 to 60 minutes, respectively. More details on the optimization of reaction time can be found in Fig. 10, Appendix. In Table 1 we summarize the results obtained for the four most relevant samples (Samples A-D of the eighteen prepared (S1-S18, Table 2 in Appendix). Table 1 specifies the process conditions and corresponding Raman results for metal-free zones in the dewetted areas (where the metal is retracted). Tables 2 and 3 in Appendix present additional data for samples A-D as well as the rest of the samples. Among the samples, those using 50 nm Ni UTMF showed improved graphene growth results in terms of quality and uniformity.
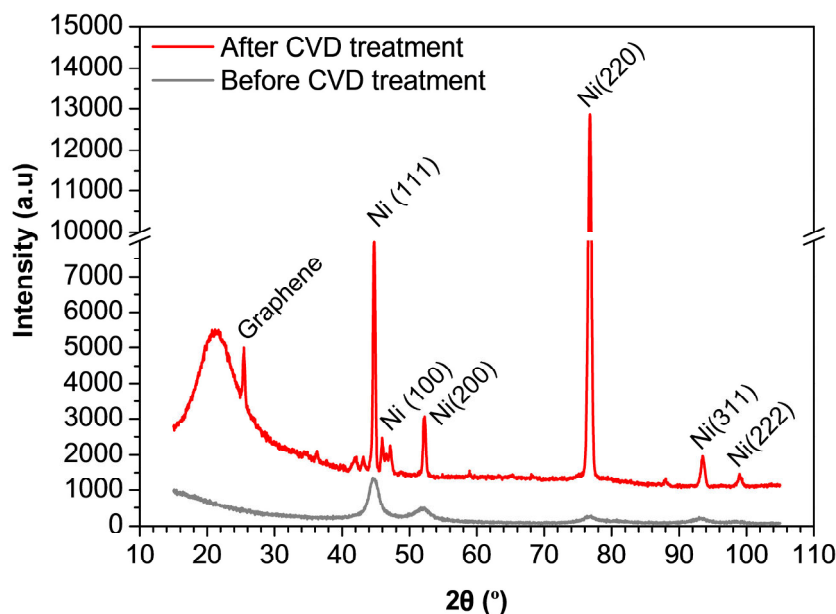

Fig. 1. GXRD spectra of 50 nm Ni UTMF at 1000°C (Sample C in Table 1) before and after CVD (grey and red lines, respectively), showing the crystallinity improvement after CVD treatment, as well as the appearance of a narrow peak at small angle associated to graphene growth.

These findings agree well with the theoretical results of ref [43], where 50 nm Ni UTMF was calculated to be the minimum thickness needed to produce SLG (see Eq. (1-2) and Table 4 in Appendix). Figure 2 shows the growth mechanism through optical microscope images of the dewetted films and Raman spectra of graphene after 30 minutes of reaction time for samples A, B and C processed at 700, 900 and 1000°C, respectively. Note that also sample S8 (50 nm, 800°C, see details in Appendix) was considered in the study, together with samples A, B and C, for a more complete and gradual evolution over the full temperature range with a single thickness (50 nm).

Table 1. Process conditions and Raman signals for graphene grown on Ni UTMF (fused silica substrate) of different thickness (Raman measurements include the ratios between graphene peaks: I_{2D}/I_G, I_D/I_G and the FWHM of 2D peak. All measurements were performed on the dewetted areas, where the metal is retracted). (Results at different conditions for same thickness are collected in Table 2 of Appendix).

		Ultrathin Ni on fused silica substrate samples			
		Sample A	Sample B	Sample C	Sample D
Process conditions	Ni (nm)	50	50	50	15
	T (ºC)	700	900	1000	1000
	t (min)	30	30	30	30
Raman results	I_{2D}/I_G	3.20±1.78	2.28 ±0.74	2.34 ±1.24	2.37 ±0.38
	I_D/I_G	0.92±0.54	0.49 ±0.46	0.17 ±0.12	0.51±0.11
	FWHM(2D) (cm^{-1})	22.8±5.74	26.8 ±2.11	26.4 ±4.98	30.1±1.65

The following stages were identified for the dewetting (purple areas correspond to Ni whereas dark areas graphene is deposited on SiO$_2$): (1) nucleation of holes at 700°C (see black dots in optical microscope image at 700°C in Fig. 2) [34], (2) enlargement of the holes for temperatures between 800 and 900°C and, (3) total retraction of the film when the temperature reached 1000°C. The dewetting evolution during CVD growth was more evident through the SEM pictures, Fig. 11 of Appendix. Raman results in Fig. 2 also pointed out the effect of temperature on graphene quality.
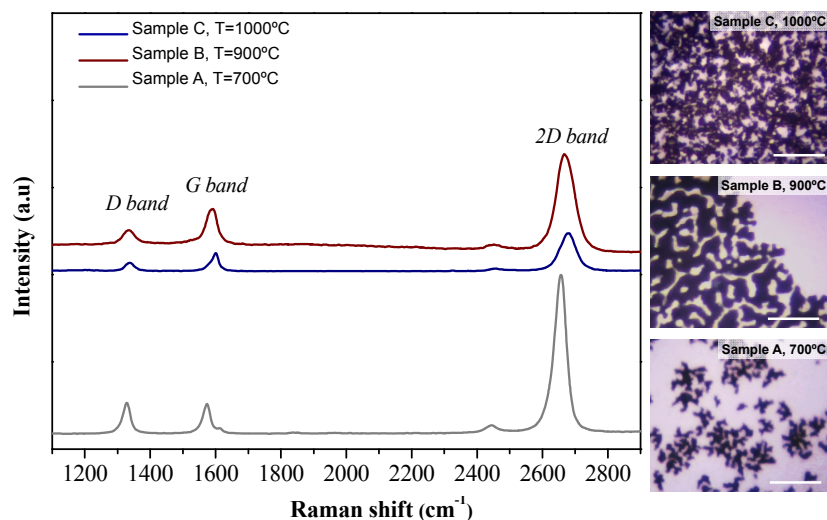
Fig. 2. Optical microscope images of 50 nm dewetted samples A, B and C after graphene growth at 700, 900 and 1000°C, respectively (for all 30 minutes reaction). Bright purple areas correspond to continuous/dewetted Ni while dark areas correspond to Ni-free regions where graphene is deposited directly on SiO$_2$. Raman spectra was measured on dewetted areas (dark) demonstrating graphene deposition on SiO$_2$. Scale bar: 10 μm.

Three characteristic peaks could be observed for all samples, corresponding to D, G and 2D bands, at 1350, 1580 and 2700 cm^{-1}, respectively. According to SLG criteria [46,47], the graphene quality can be measured in terms of: intensity ratios between D peak and G peak (I_D/I_G), whose value should be very low as D peak is related to material defects; intensity ratios between 2D peak and G peak (I_{2D}/I_G), whose value should be equal or higher than 2; and the full width at half maximum of 2D peak (FWHM (2D)), which varies depending on

whether it is exfoliated or CVD grown graphene. For example, for exfoliated graphene this value should be in the 25-30 cm^{-1} range while for CVD graphene it is typically larger. Best results were obtained at 700°C for graphene grown on the nucleation holes resulting in I_{2D}/I_G of 3.20 (Sample A). SLG with high quality was also obtained on dewetted regions at 900 and 1000°C with I_{2D}/I_G ratios of 2.28 and 2.37, respectively. A difference in graphene's quality in terms of I_{2D}/I_G ratio was noticeable between measurements of dewetted areas with and without Ni particles (as reported for Sample B). According to ref [48], defect lengths (L_D) were calculated for graphene grown on dewetted areas (see Eq. (3) in Appendix) giving values in the 12.4-23.7 nm range, which were higher than those previously obtained for dewetted Cu thin films [17].

In the following subsections, we present the most significant and representative results and the different regimes of graphene growth as a function of process temperature for samples A-D. Results for other samples performed at different conditions of thickness, temperature and reaction time can be found in Appendix, which are necessary for further understanding of the growth mechanism of graphene.

Growth at 700°C A very peculiar graphene growth occurred at 700°C for films of 50 nm thickness (Sample A). Due to low temperature, dewetting was very slow and only nucleation of irregular holes in the film appeared. Over the holes, suspended graphene started to grow in patches that could reach around 2 μm^2 area as shown by the SEM image in Fig. 3(a), where the wrinkled area corresponds to graphene. Atomic Force Microscopy (AFM) images in Fig. 3(b-d) show a hole (marked by green dotted line) also partially covered by graphene. The height profile cross sections of the graphene (Fig. 3(d)) and the abrupt change in phase for the AFM signal (Fig. 3(c)) confirm that graphene was suspended about 90 nm over the glass surface free of any metal. Figure 12 (Appendix) shows Raman maps of 10x10 μm^2 with well delimited patches of graphene on the metal-free dewetted Ni film areas. SLG growth was confirmed by the high I_{2D}/I_G ratio and single sharp Lorentzian-shape of the 2D band with FWHM (2D) = 25-30 cm^{-1}, typical evidences of SLG [46,47]. In addition, the centers of the 2D and G peaks were slightly shifted compared to the typical values for SLG grown on standard Cu foils (2673 cm^{-1} and 1582 cm^{-1}, respectively as shown in Fig. 12 and Fig. 13(a)-13(b) in Appendix. Apart from the presence of defects confirmed by the appearance of the D peak, the shifts and broadening of the 2D peak can be attributed to strain in graphene due to the effect of the Ni grain boundaries and residual stress in the Ni film after graphene growth [14]. An average L_D = 14.4 nm for Sample A is calculated from Raman spectra (Fig. 12). Moreover, Rs measurements from 4-point probe system gave very low values (see Appendix) because of the contribution of Ni underneath graphene.
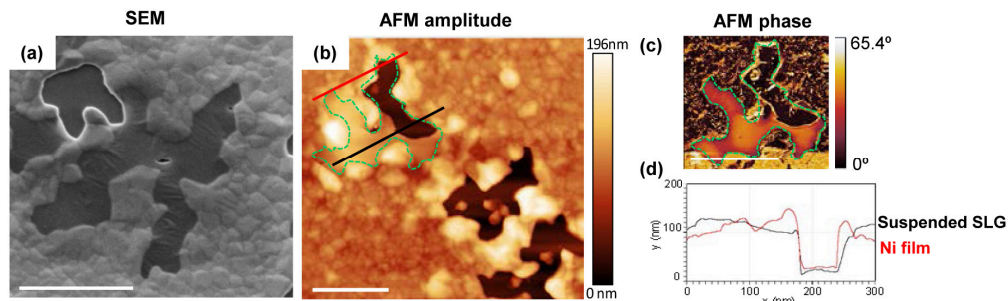

Fig. 3. Growth of suspended graphene on dewetted Ni holes (Sample A). (a) SEM image of a hole partially covered by suspended graphene, identifiable by the wrinkles; (b) AFM amplitude and (c) phase images of graphene suspended over a hole, different from that of the SEM image in (a). The green dotted line indicates the hole's borders. (d) Cross sections of the AFM amplitude map corresponding to Ni continuous film only (red line) and suspended graphene (black line). In all figures the scale bar is 2 μm.

Growth at 800°C The results are in Table 2 of Appendix.

Growth at 900°C At the temperature of 900°C, Ni films partially dewetted leaving, after metal retraction, a uniform graphene layer covering the whole sample. To illustrate the differences in graphene properties between the dewetted and non-dewetted (still continuous metal film) areas, Fig. 4(a) shows the Raman spatial distribution of a $20x20$ μm^2 area across these two regions in 50 nm Ni film (Sample B). The metal edges were determined from the optical microscope image (see Fig. 13(d) in Appendix) and superimposed as a reference. In the dewetted region, the graphene was almost entirely uniform and of good quality, in contrast to that in the continuous Ni film region. Similarly to what reported in ref [17], a higher quality graphene was present in the metal-free dewetted area. In Fig. 4(d) we report the statistics distribution separately collected over the two regions. In the dewetted region, SLG grew with a single and sharp Lorentzian peak of the 2D band, FWHM (2D) value = 25-30 cm^{-1} with L_D = 13.9 nm, while the other region presented a FWHM = 40-45 cm^{-1} over a very broad range. In addition, AFM measurements (Fig. 14 in Appendix) revealed graphene wrinkles with a height of 1-5 nm close to the continuous film area as well as graphene domains with a size ranging from 130 nm to 410 nm. Rs measurements from 4-point probe system gave very low values (see Appendix) when measuring on non-dewetted area because of the contribution of Ni underneath graphene, but however, on the dewetted area, Rs could not be measured likely due to the high roughness of Ni particles. Although 50 nm was the optimum thickness for best quality of graphene, the case of 5 nm Ni film at 900°C (sample S9) is commented due to interesting results. The SEM picture of Fig. 15(a) in Appendix, reveals that complete dewetting occurred and small Ni nanoparticles with an average diameter of about 200 nm remained on the whole surface. While Raman mapping showed low I_{2D}/I_G values indicating few-layer graphene, the Rs = 34.2 kΩ/sq indicated the presence of a continuous conducting layer over the whole area. Indeed, except for a tiny hole in the central part of the SEM picture (Fig. 15(a)), the graphene film was continuous over the whole sample. Graphene deposited under these conditions exhibited a high I_D/I_G ratio, which could be related also to the presence of Ni nanoparticles and the fast dynamics of metal retraction occurring at 900°C for 5 nm thick Ni, then affecting also to the high Rs. Also, an L_D value of 12.4 nm was obtained.
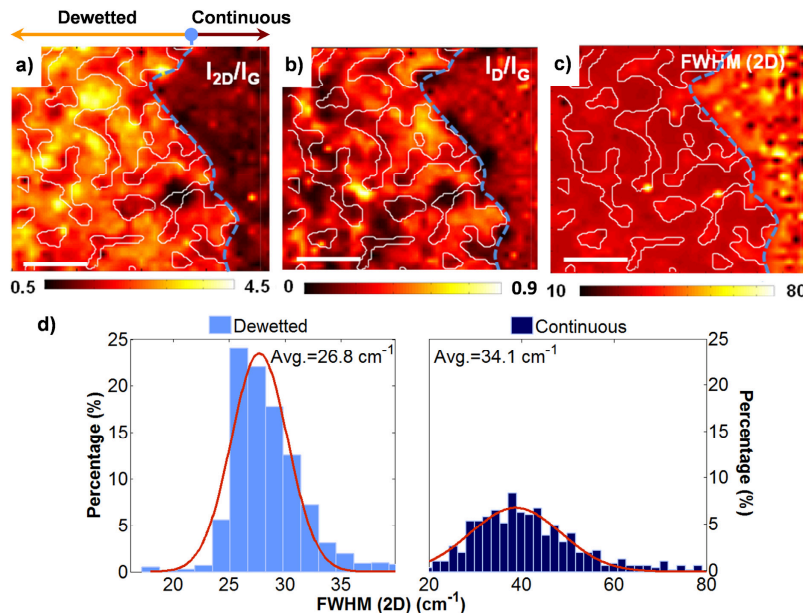

Fig. 4. Raman maps of Sample B (50 nm/900°C) show (a) high I_{2D}/I_G ratio of SLG grown on the dewetted area, (b) I_D/I_G ratio map, and (c-d) FWHM of 2D peak and statistics for both areas (See original optical microscope image (Fig. 13(d)) and AFM measurement (Fig. 14), in Appendix. Scale bar: 5μm.

Growth at 1000°C At a process temperature of 1000°C, for both 50 and 15 nm films thicknesses, samples C and D, respectively, graphene with high I_{2D}/I_G Raman ratio was grown in the retracted metal regions, as confirmed by Raman maps (Fig. 15(c) and Fig. 15(b)), where the I_{2D}/I_G ratio is high and fairly constant. For both thicknesses, the 2D band fitted to a sharp and single Lorentzian peak with FWHM values = 27-30 cm^{-1} and L_D = 17.4 and 23.7 nm, respectively. Rs was measured for Sample D (about 8 kOhm/sq) while it could not be measured for sample C, most likely due to the high roughness associated to Ni particle remains.

To compare the results for the different growth conditions described above, we show in Fig. 5 the percentage of the areas covered by graphene versus graphene quality in terms of I_{2D}/I_G ratio (Raman mapping). Percentages include areas with presence of 2D peak and with I_{2D}/I_G ratio in the 0.1-4.8 range. For all samples, we can conclude that graphene compounds covered up to 95% of the total area. The SLG coverage varied significantly from sample to sample. The large variation is in part associated to a measurement artifact, i.e. the fact that the presence of Ni affects Raman measurements. Regardless, one can affirm that sample B presents higher quality SLG graphene, among the samples investigated. For more definitive conclusions on the quality we shall consider the electrical and optical results after Ni removal.
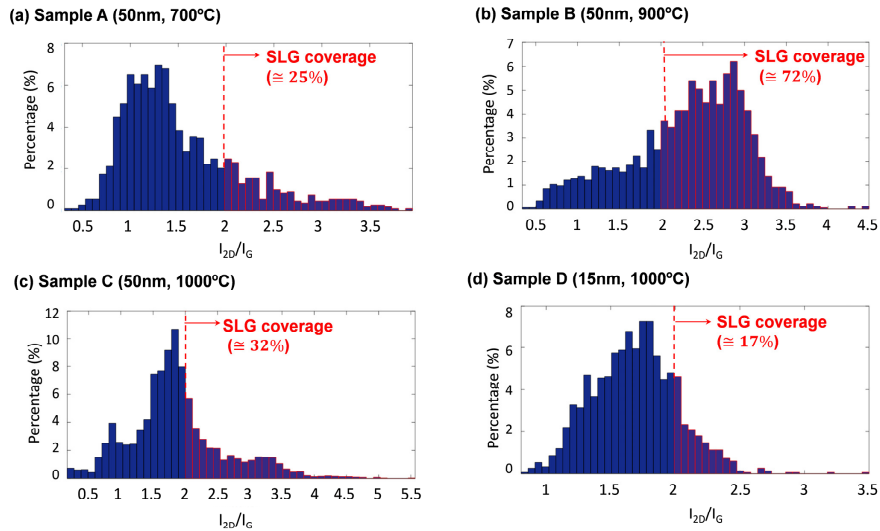

Fig. 5. Percentage of graphene coverage versus quality, i.e. I_{2D}/I_G from Raman maps of: (a) Sample A, (b) Sample B, (c) Sample C and (d) Sample D. Note that the presence of Ni particle remains affect the Raman measurements, so the data are only indicative.

In Fig. 6 we propose a qualitative model of graphene growth on Ni-UTMF. During the heating phase (a), the Ni-UTMF experiences an increase in grain size and improvement in crystallinity with preferential (111) and (220) orientations [12,44]. At a certain temperature, the dewetting nucleation (b) starts with the appearance of holes and their subsequent propagation. Already during this stage, upon retraction of the Ni film, graphene starts growing. While the temperature increases (e.g. to 1000°C), dewetting proceeds further while graphene continues to deposit on the substrate, this until the system cools down (c).
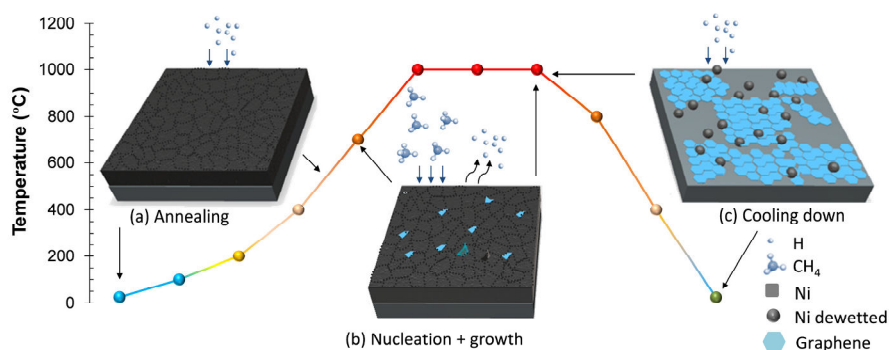
Fig. 6. Schematic model of graphene growth on 50 nm Ni UTMF: (a) first step of annealing, where activation, reduction and crystallization take place, (b) nucleation of holes promoting Ni dewetting and deposition of graphene upon metal retraction starting at 700°C and (c) cooling down where graphene is already deposited on the silica substrate.

4. Applications

For many applications, especially involving the use of light (optical and optoelectronic devices), transparency is crucial. Ni is responsible for most of the optical loss, thus has to be completely removed after graphene growth is finished. Different removal approaches can be employed, including thermal evaporation [49] or wet chemical etching. While in some cases the thermal evaporation could be effective to completely remove Ni residues, the required vacuum conditions and high temperatures (>1100°C) make it unsuitable for many substrate materials, for example low strain point glasses. For this reason, we preferred a diluted aqua regia solution (5-15 minutes duration). After Ni etching, we believe that graphene deposited on glass is originated from the top side of the Ni for Sample A, where graphene is growing on dewetted holes. However, for samples B, C, and D, graphene could have originated from the bottom side of Ni. In these cases, higher temperatures could improve the absorption of carbon inside the metal. Additionally, as the Ni film is dewetted, the catalyst surface area in contact with the carbon source would be larger, with more active sites where carbon could be absorbed. A visible evolution in the transmission and absorbance values at 550 nm are observed in Fig. 7(a)-7(b) for samples A, B, C and D, before and after Ni removal. Absorbance measurements were obtained by measuring transmittance (T) and reflectance (R) of samples with the spectrophotometer, and then calculating absorbance (A) as: A = 100-T-R. Evolution in transmission is also shown in Fig. 7(c) through a series of pictures for exemplary samples A and C. All the results confirm a significant recovery of the samples' transmittances. In particular, sample A reached 91.07% transmission (average value over the 400-700 nm wavelength range), indicating an optical loss of 2.38% with respect to the bare fused silica substrate, also represented in the figure with a measured transmittance of 93.45%. The optical loss is thus very close to the expected absorption of a SLG (2.3%). More complete transmittance spectra are shown in Fig. 16 (Appendix).
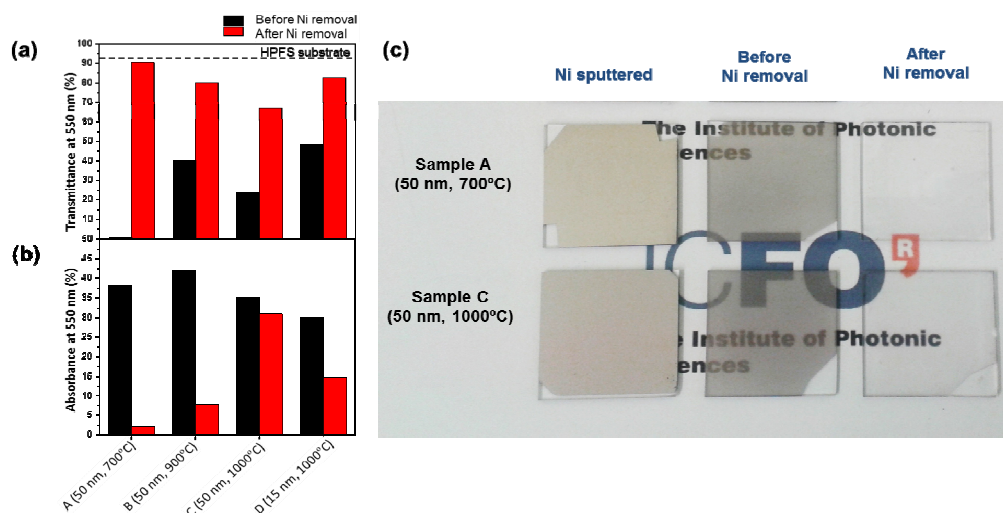
Fig. 7. (a-b) Transmittance (including substrate contribution) and absorbance values at 550 nm of samples A-D before (in black) and after (in red) Ni removal. (c) Picture of Sample A and Sample C (Ni 50 nm at 700°C and Ni 50 nm at 1000°C, respectively) as deposited (first column), after graphene growth (second column) and after Ni removal (third column).

In order to demonstrate the potential for applications of the proposed technique, we produced ribbons and square patterns of graphene directly grown on conventional SiO_2 on Si substrates and low strain point temperature glass, such as ultrathin and flexible 100 μm thick Willow® Glass (Fig. 8(a)-8(b) and Fig. 8(e)-8(f)) at the same conditions than sample A. An efficient direct growth on Willow® Glass [50] would enable large scale and roll to roll production of transparent substrates with graphene for flexible electronics and optoelectronics. Ni 50 nm patterns of different size (ranging from 500 nm to 1 mm) were first sputtered. Graphene was then grown on the substrates at 700°C for 30 minutes. Finally, Ni was removed by dipping the samples in diluted aqua regia for 5-10 minutes (Fig. 8(b) and Fig. 8(f)). For all patterns, graphene was continuous over the substrates as indicated by SEM characterization (Fig. 8(c) and Fig. 8(g)-8(h)) and Raman maps (Fig. 17 in Appendix). Also, EDX measurements revealed that graphene was free of Ni residues (see Table 5 in Appendix). For graphene electrical characterization, Au contact pads were deposited via evaporation on graphene corners (see Fig. 8(d)) to perform 4-point probe measurements, obtaining Rs values of about 2 kOhm/sq.
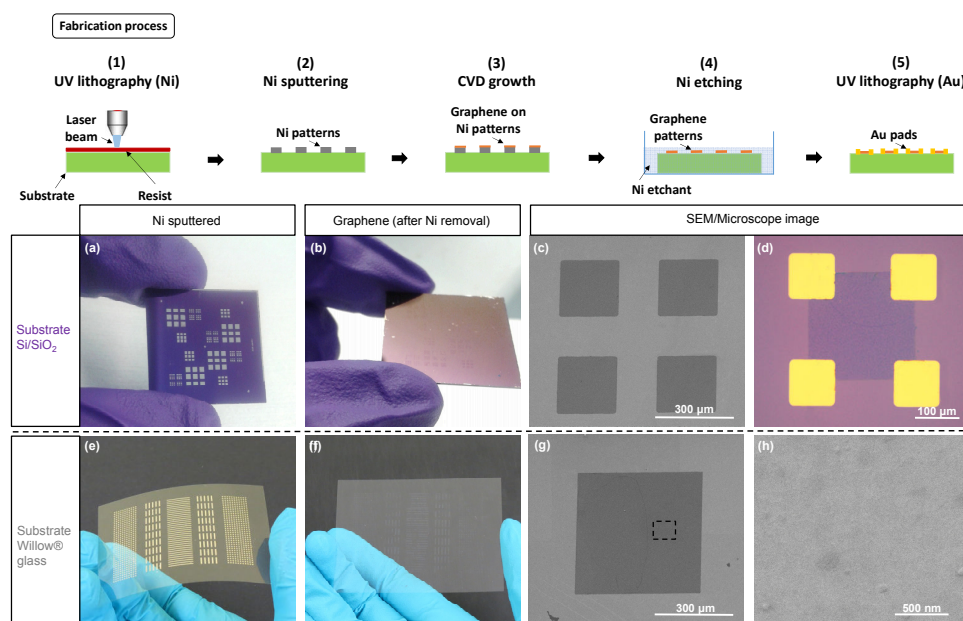
Fig. 8. Flow chart on top shows different steps for graphene patterns fabrication (see more details in section 2.1). Optical images of Ni 50 nm UTMF patterned on Si/SiO$_2$ and Corning® Willow® Glass substrates in square shapes of different size (a,e) as deposited via sputtering and (b,f) after Ni removal when graphene is deposited at the same condition than Sample A. SEM images in (c, g-h) show high quality graphene squares after Ni removal with absence of any metal residues and holes (also EDX results in Table 5 in Appendix) for both substrates. Au electrodes for 4-point probe measurements are shown in (d).

5. Conclusions

In summary, the use of Ni UTMF as a catalyst, template and sacrificial layer can lead to a fast and high quality formation of graphene directly on a glass substrate, at minimum temperatures of 700°C. We performed a systematic study of Ni UTMFs dewetting, as well as of the effect of Ni dewetting on graphene growth, pointing out that dewetting dynamics, strongly affected by temperature, are very important to achieve high percentage area coverage with graphene. With soft etching of the residual Ni, the substrate with graphene regained very high transparency, still maintaining good electrical conductivity. The technique thus widens the range of substrate materials on which graphene can be directly grown, avoiding in this way costly, cumbersome and not always defect-free transfer techniques. This has already been demonstrated by growing graphene patterns on ultrathin glass, a functionalized substrate with great potential for flexible electronic and optoelectronic devices.

APPENDIX:

Graphene deposition

After depositing the UTMF on top of the fused silica, the substrate is placed in the PE-CVD chamber (Black Magic 4-inch, AIXTRON). At low pressure, a pre-treatment with H$_2$ is carried out before starting the growth. Thus, a double action takes place at the metal catalyst surface: a redox chemical reaction where possible metal oxides forming at the surface are reduced to their active phase (fundamental state: Ni^0), and an increase of the grain size leading to a reduction of the material defects. When temperature stabilizes, the reaction gases are fed into the system (CH$_4$/ H$_2$: 30/20 sccm). Finally, the samples are cooled down under a continuous flow of H$_2$ in order to remove amorphous carbon from the surface.

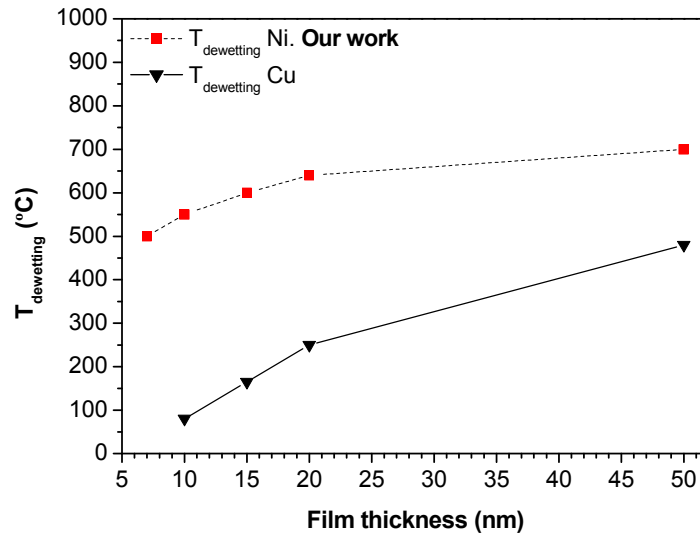Fig. 9. $T_{dewetting}$ as a function of different UTMF thicknesses for Ni (our work) and Cu [41,42], dashed and solid line, respectively.

Reaction time optimization dependence of graphene growth

To evaluate the effect of time in graphene deposition, some quality tests, in terms of I_{2D}/I_G ratios and FWHM 2D values, were performed at 15, 30 and 60 minutes reaction time for 5 and 50 nm Ni UTMF. Results in Fig. 10(a)-10(b) reveal that, for different thicknesses and temperatures, 30 minutes was the optimum time, giving the highest I_{2D}/I_G ratios and lowest FWHM 2D values, still within SLG ranges (shaded areas in the graphs). The general tendency was that, for 15 minutes of reaction time only, samples were characterized by low I_{2D}/I_G ratios (high FWHM 2D values), which may be attributed to an incomplete formation of graphene (2D band is very low and broad). For 30 minutes, the quality was improved as confirmed by an increase in I_{2D}/I_G ratios (decrease in FWHM 2D values). Finally, for 60 minutes, the I_{2D}/I_G ratios decreased (FWHM 2D increased). This may indicate that as time increases, more carbon is absorbed and segregated upon metal retraction, thus promoting the growth of MLG.
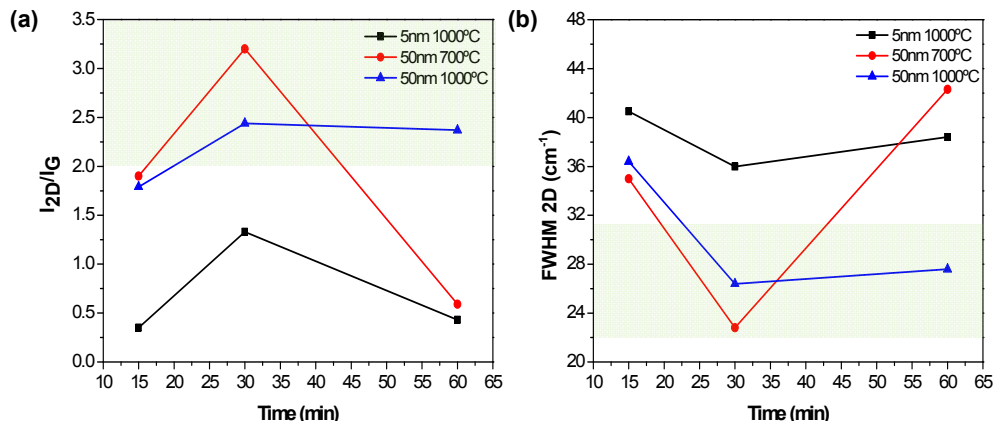

Fig. 10. Reaction time effect on graphene quality evaluating (a) I_{2D}/I_G and (b) FWHM 2D peak, at 15, 30 and 60 minutes, respectively. Shaded area corresponds to values for theoretical SLG.

Table 2. Process conditions and Raman/electrical results for graphene deposited on Ni UTMF

	S1	S2	S3	S4 (A)	S5	S6	S7	S8	S9	S10	S11 (B)	S12	S13	S14	S15 (D)	S16 (C)	S17	S18
Ni (nm)	5	15	50	50	50	5	15	50	5	15	50	5	50	5	15	50	5	50
T (°C)	700	700	700	700	700	800	800	800	900	900	900	1000	1000	1000	1000	1000	1000	1000
t (min)	30	30	15	30	60	30	30	30	30	30	30	15	15	30	30	30	60	60
ω_{2D} (cm⁻¹)	2665.5	2684.5	2676.3	2657.3	2698.3	2680.2	2678.8	2706.2	2676.6	2674.9	2681.4	2679.7	2675.9	2663.8	2664.6	2667.2	2666.1	2657.9
ω_G (cm⁻¹)	1592.5	1600.9	1592.4	1574.6	1578.5	1598.6	1600.5	1585.5	1594.6	1600.8	1603.5	1588.9	1596.2	1577.2	1593.5	1589.6	1593.5	1586.1
ω_D (cm⁻¹)	1335.6	1345.5	1332.5	1329.3	1351.5	1342.0	1341.1	1354.1	1344.9	1342.3	1338.0	1341.7	1335.9	1335.0	1336.6	1333.9	1340.9	1333.9
I_{2D}/I_G	0.04 ±0.04	0.09 ±0.06	1.9 ±0.22	3.20 ±1.78	0.59 ±0.12	0.16 ±0.03	0.36 ±0.08	0.53 ±0.27	0.38 ±0.06	1.20 ±0.28	2.28 ±0.74	0.35 ±0.08	1.79 ±1.30	1.33 ±0.09	2.37 ±0.38	2.44 ±1.24	0.43 ±0.03	2.39 ±0.49
I_D/I_G	0.62 ±0.33	0.93 ±0.07	1.22 ±0.11	0.92 ±0.54	0.36 ±0.21	0.96 ±0.07	1.07 ±0.16	0.25 ±0.20	0.95 ±0.13	1.11 ±0.13	0.49 ±0.46	0.90 ±0.11	0.91 ±0.44	0.87 ±0.07	0.51 ±0.11	0.17 ±0.12	1.25 ±0.06	0.53 ±0.27
FWHM (2D)	44.7 ±2.41	42.2 ±3.78	35.3 ±2.34	22.8 ±5.74	42.3 ±2.48	41.15 ±3.79	43.94 ±3.51	35.57 ±0.62	43.8 ±3.65	42.0 ±1.25	26.8 ±2.11	40.5 ±2.85	36.4 ±4.22	36.0 ±2.56	30.1 ±2.37	26.4 ±4.98	38.4 ±2.26	27.6 ±3.34
Rs [b] (kΩ/sq)	54.0	52.8	1.2·10³ [c]	1.4·10³ [c]	1.5·10³ [c]	52.4	83.4	2·10³ [c]	34.2	16.8	1.7·10³ [c]	58.9	-	17.55	8.16	-	16.9	-

[a] Conditions for all samples: P = 7 mbar, CH₄/H₂ = 1.5, %N₂ = 0 and %Ar = 0.

[b] Note that Rs measurements were performed with the 4-point probe system measuring directly on the graphene/Ni surface. Residual Ni affects the measurements. Also, at 1000°C, the high roughness of Ni/graphene surface makes difficult a correct evaluation of Rs.

[c] Ni film was almost continuous as the dewetting of the film was at the initial nucleation state. In sample B, Rs was measured on continuous Ni film.

Table 3. Raman measurement results on UTMF Ni of different thickness. (Raman measured on the non-dewetted areas).

	Sample A	Sample B	Sample C	Sample D
I_{2D}/I_G	1.24 ± 0.45	1.36 ± 0.68	1.73 ± 0.85	1.57 ± 0.30
I_D/I_G	0.82 ± 0.37	0.88 ± 0.39	0.29 ± 0.16	0.57 ± 0.21
FWHM 2D (cm^{-1})	32.6 ± 4.45	34.1 ± 10.6	28.2 ± 2.72	31.7 ± 1.59

Graphene layers calculation (adapted from ref. 43)

The theoretical number of graphene layers grown from a Ni catalyst can be calculated. Two different processes occur when using Ni as a catalyst template (precipitation and segregation during the cooling down),

$$S(GLs) = \frac{S\left(atoms \cdot cm^{-3}\right) \cdot L_{NiUTMF}}{\rho_{GrapheneAtomicLayer}} \quad (1)$$

where:

$S(GLs)$: Solubility in graphene layers (atoms·cm^{-3})

S: Carbon solubility in nickel (atoms·cm^{-3})

L_{NiUTMF}: Thickness of Ni UTMF (cm)

$\rho_{GrapheneAtomicLayer}$: Graphene atomic layer density = 3.8·1015 (C atoms·cm^{-2})

$$S = S_O \cdot \exp\left(\frac{H_P}{k \cdot T}\right) \quad (2)$$

where:

S_O: Entropic pre-factor related to the density of sites where solute atoms sit = 5.33 (atoms·cm^{-3})

H_P: Heat of precipitation = −0.421 eV

k: Boltzmann's constant = 1.38·10^{-23} m^2 kg·s^2 K^{-1}

T: Temperature (K)

Table 4. Graphene layers calculation of different Ni films treated at different temperatures

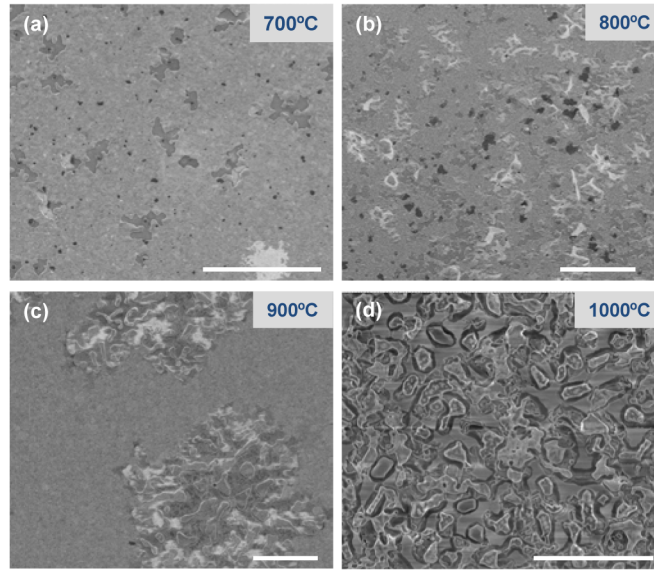| Ni thickness (nm)	S(GLs) from Eq. (1)			
	Temperature (°C)			
	700	800	900	1000
5	0.05	0.07	0.11	0.15
15	0.14	0.22	0.33	0.45
50	0.46	0.74	**1.09**	**1.51**

Fig. 11. SEM pictures of Ni 50nm at 700°C, 800°C, 900°C, 1000°C (sample A, S8, sample B and sample C) showing the dewetting evolution when the process temperature is raised: (a) nucleation step of holes, (b-c) holes propagation and (d) total dewetting of the Ni UTMF. Scale bar: 10μm

Defect length (L$_D$) calculation (adapted from ref. [48])

$$L_D^2(nm^2) = 5.4 \cdot 10^{-2} \cdot E_L^4(eV^4) \cdot (I_D/I_G) \qquad (3)$$

where:

E$_L$: Laser excitation energy = 2.33 eV

I$_D$/I$_G$: Ratio calculated from Raman maps
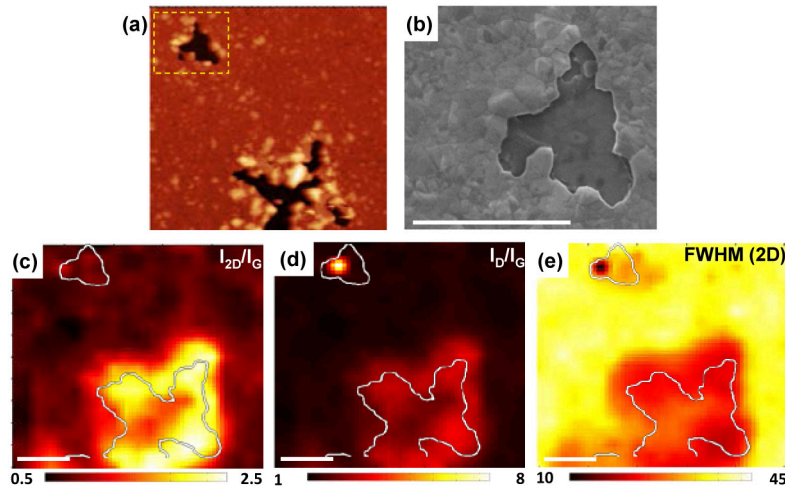
Fig. 12. Sample A (700°C, nucleation step): (a-b) AFM and SEM pictures showing the holes formed at the beginning of the dewetting (b) corresponds to the yellow dashed area in (a), (c-e) Raman maps of the area in (a) demonstrating graphene coverage on the holes, as I$_{2D}$/I$_G$ ratios are very high, and FWHM 2D values are within 25-30 cm^{-1}, values assigned to SLG. Scale bar: 2 μm.
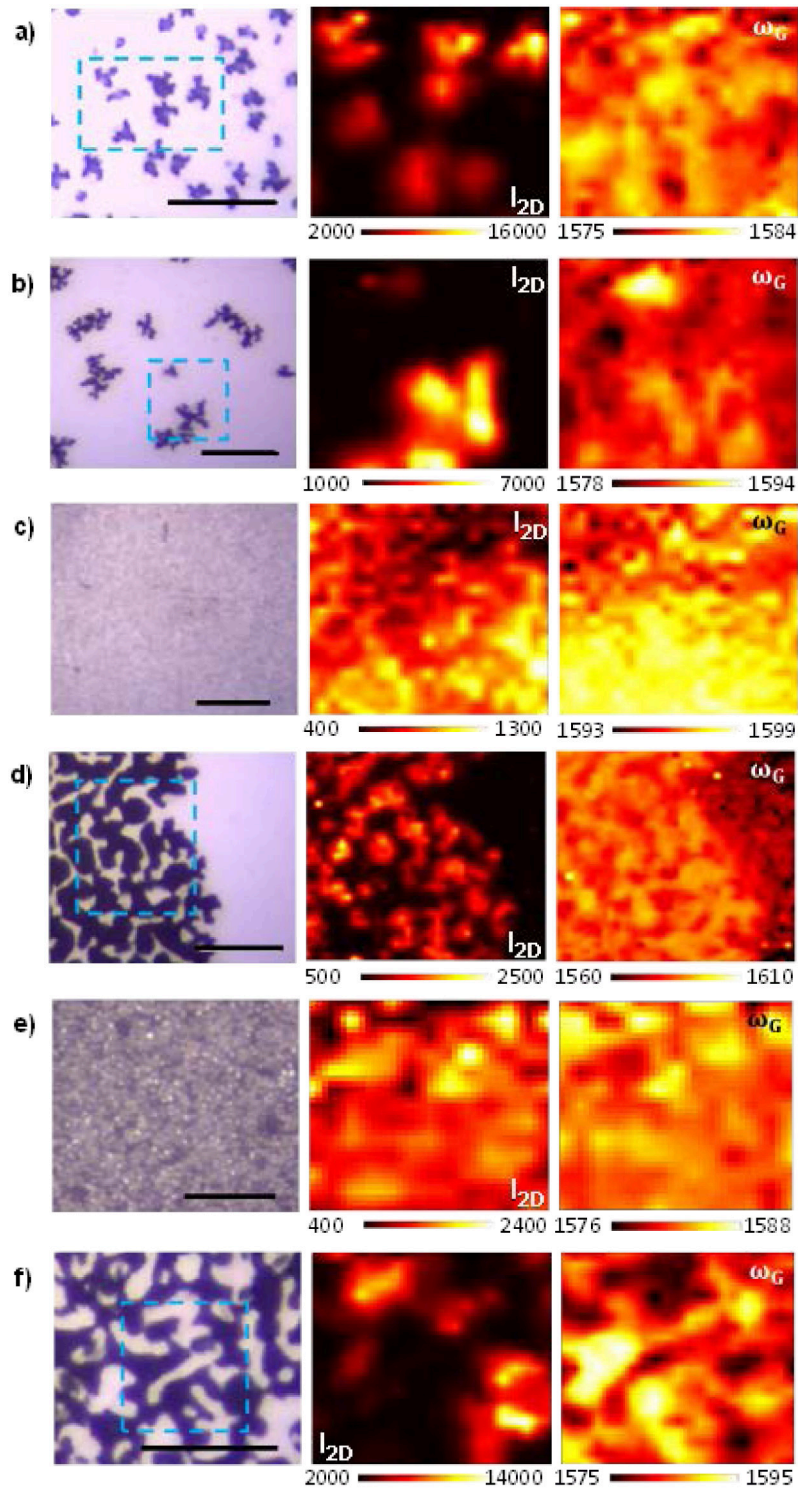
Fig. 13. Optical microscope image and I_{2D} and shift of the G peak. (a-b) gives Raman maps (10x10 μm^2) for two different regions of Sample A (blue squares), (c) S9, (d) Sample B, (map of the region within the blue square), (e) Sample D and (f) Sample C (map of the region within the blue square). Scale bar: 10μm.
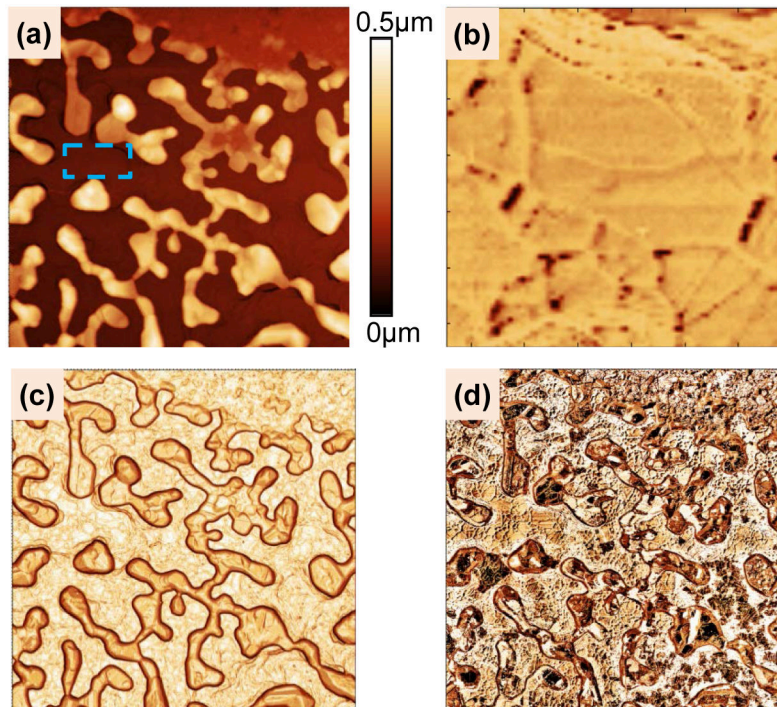
Fig. 14. AFM measurements of Sample B: (a) height map, (b) zoomed area from (a) (blue dashed square) showing the graphene domains, (c) height map with increased contrast to enhance the ripple and domain structures of graphene grown on SiO_2 after metal retraction, and (d) phase map. (Map: 15x15 μm^2).
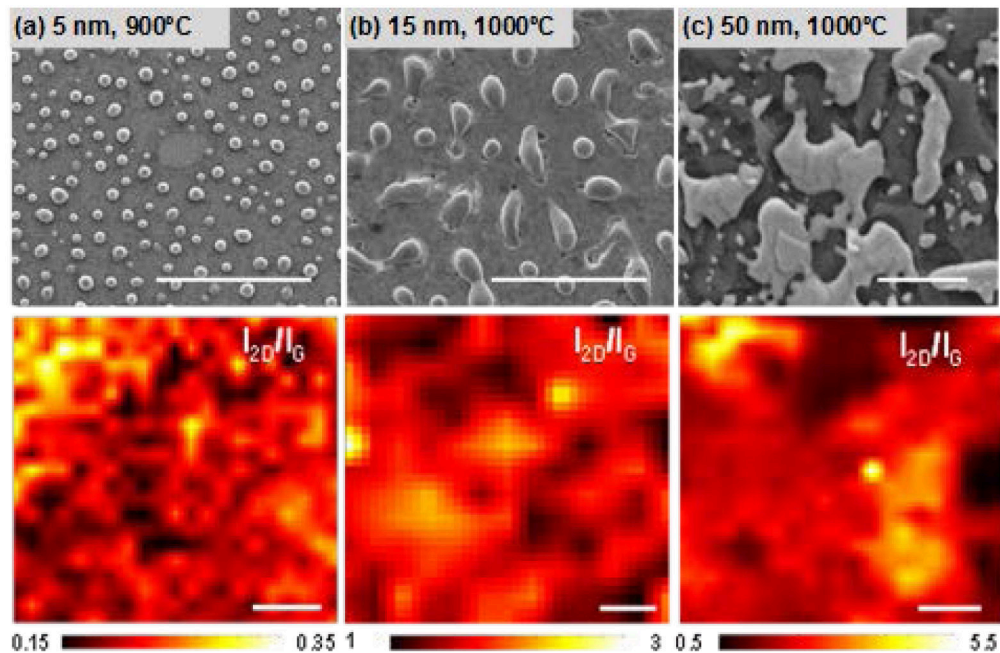
Fig. 15. SEM images and Raman maps of I_{2D}/I_G of graphene grown on different Ni thicknesses and at different temperatures (all 30 minutes reaction time): (a) S9 (5 nm, 900°C), (b) Sample D (15 nm, 1000°C) and (c) Sample C (50 nm, 1000°C). Scale bar: 2μm.
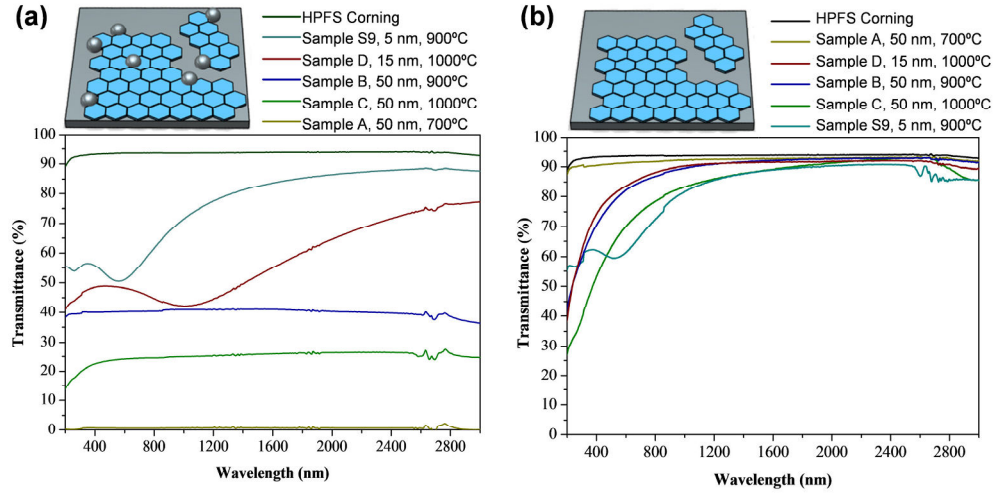
Fig. 16. Transmittance spectra of highest quality UTMF Ni samples: (a) after CVD processing and (b) after etching process of 15 minutes.
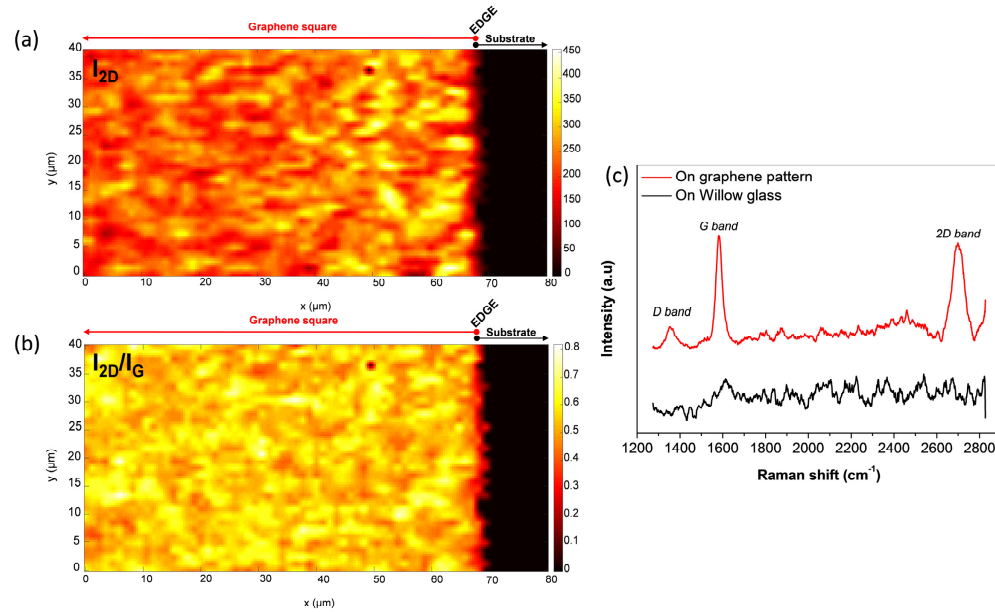

Fig. 17. Raman mapping of graphene square patterned on willow glass: (a) I_{2D} peak, (b) I_{2D}/I_G ratio and (c) Raman spectra when measuring inside and outside of the pattern region.

Table 5. EDX measurements on graphene after Ni removal from Sample A

| | Atomic percentage detected by EDX technique ||
	On graphene	On residues
Carbon	44.79	48.07
Oxygen	29.63	29.54
Silicon	25.99	22.52
Nickel	-	-

Acknowledgments